

## Chapter 7

# Molecular magnetism induced by charge transfer on TTF-TCNQ

The organic conductor TTF-TCNQ is a bulk weak paramagnet at room temperature [169, 170]. Its magnetic susceptibility depends strongly on the temperature. Below 54 K it exhibits a strong decrease due to the opening of energy gaps at the metal-insulator phase transition [169] and disappears completely in the TCNQ chains for temperatures approaching 0 K [127]. Therefore, the strong anisotropy of the bulk crystal given by the quasi 1D chains, together with the Peierls instabilities taking place in these chains, reduce drastically the molecular paramagnetism of the material for low temperatures. Hence, bulk TTF-TCNQ can not be considered a magnetic material for sufficiently low temperatures.

However, as shown in the previous chapter, TTF-TCNQ self-assembles in the ultra-thin film regime in molecular rows in similarity to the crystal, but exhibiting a planar adsorption that introduces new properties at the interface. In particular, we find the transfer of one electron from TTF to TCNQ (Section 6.2.1), in contrast to the  $0.59 e^-$  charge transfer reported in bulk. This charge donation occurs even in the presence of an underlying metallic surface, and causes a shift of the non-degenerated LUMO of the TCNQ towards the Fermi level. Thus, the LUMO becomes a singly occupied orbital (see Fig. 6.7(a)). Furthermore, the TCNQ has been shown to be weakly adsorbed on the surface. Consequently, its electronic structure is almost unperturbed by the surface and the unpaired electron is localized in the TCNQ molecule. As a result, TCNQ becomes a magnetic molecule upon charge transfer, even though it is formed by non-magnetic atoms.

In order to prove the magnetic state of TCNQ we employ LT-STs. Ideally, the perfect tool for probing the magnetic nature of TCNQ in the molecular ensemble would be Spin-polarized STM [171, 172]. Here we demonstrate the magnetic state of TCNQ molecules in a TTF-TCNQ layer using another spectroscopic fingerprint also related to magnetism at low temperatures: the Kondo effect.

## 7.1 Brief introduction to spin Kondo effect

The spin Kondo effect is a many-body problem that arises from the interaction between a single magnetic atom/molecule with an intrinsic spin and the electrons (spins) in a non-magnetic material. The motivation for the development of this theory lies in the search of an explanation for the conductivity behavior of metals with magnetic impurities. The resistivity of a pure metal decreases with the temperature due to electron-phonon scattering, stabilizing at a minimum value that remains constant below a critical temperature. Such value depends on the amount of defects/impurities of the metal that act as scattering centers. In the case of a metal doped with magnetic impurities, this low-temperature resistance increases below a certain temperature value (known as Kondo temperature). This behavior was explained by Kondo, considering the scattering from a magnetic ion that interacts with the spins of the conducting electrons.

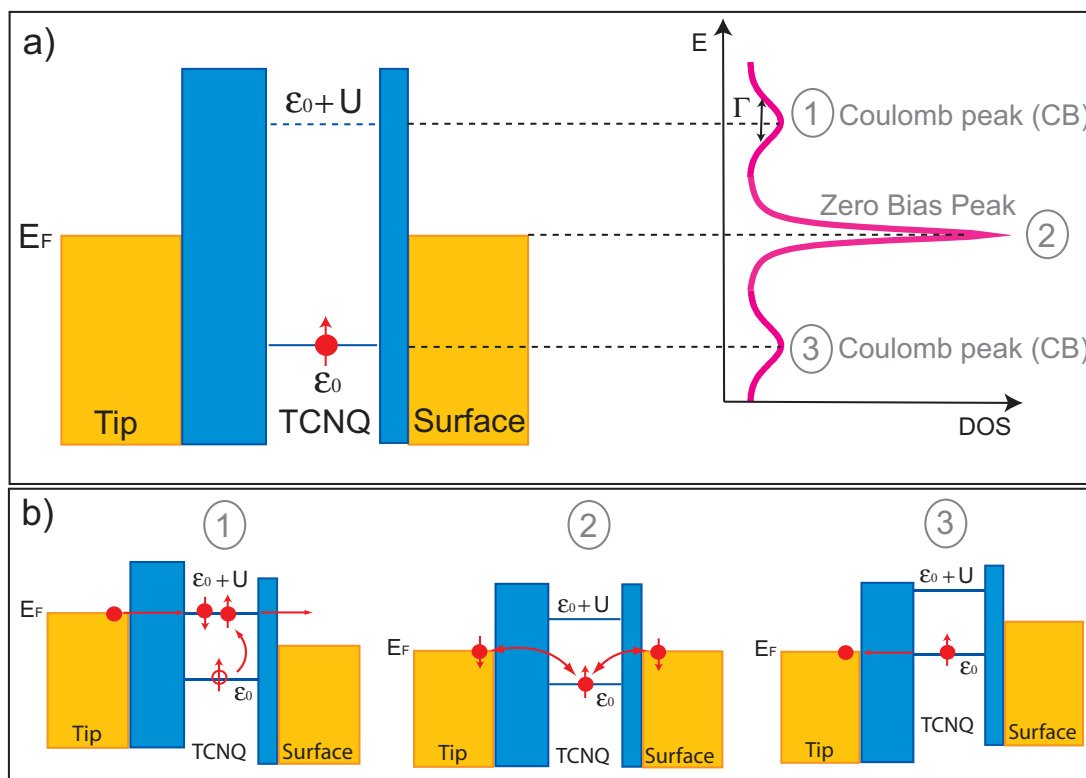


**Figure 7.1:** (a) Scheme of the density of states expected in the exchange process. The central peak at Fermi (ZBP) arises from the spin-flip mechanism and the Coulomb peaks (CB) correspond to the occupation of resonances  $\epsilon_0$  and  $\epsilon_0 + U$ . (b) Schemes of the tunneling processes leading to the resonances of (a). 1 and 3 represent resonant tunneling through  $\epsilon_0$  and  $\epsilon_0 + U$  Coulomb peaks. 2 represents the spin-flip that occurs via virtual bound states at the Fermi level of the electron sea.

The physics involved in the Kondo problem can be understood from the perspective of the Anderson impurity model, which was developed to explain the formation of mag-

netic moments in a metal [173]. The simplest Anderson model features the interaction of one local moment related to a magnetic impurity and the host electrons in the metal. As sketched in Fig. 7.1,  $\epsilon_0$  is the energy of the resonance where the electron is located. The addition of an extra spin in the local state  $\epsilon_0$  costs an extra energy  $U$ , related to the Coulomb repulsion between the two charges. For sufficiently low temperature, exchange processes that effectively flip the spin of the impurity can take place. This exchange implies the creation of a bound state with electrons in the Fermi sea of the host metal. The spin-flip processes occur via virtual intermediate states whose lifetime is large enough and provide the sufficient energy for the spin to jump between the local state and the electron sea as sketched in Fig. 7.1(b). The exchange process occurs at the Fermi level of the metal. As a consequence of the spin-flip of electrons between the impurity and the metallic Fermi sea at  $E_F$ , the density of states increases at this energy value forming the so-called Kondo-Abrikosov-Suhl resonance or zero bias peak (ZBP). The extra Coulomb Blockade (CB) peaks appear by resonant tunneling processes when either the Fermi level of the tip or the surface are aligned with the molecular levels  $\epsilon_0$  or  $\epsilon_0 + U$  (Fig. 7.1).

The Anderson model has several regimes. The parameters that rule the transitions between the different scenarios are i) the energy of the magnetic impurity state,  $\epsilon_0$ , ii) the Coulomb repulsion  $U$ , and iii) the typical resonance width  $\Gamma$ . The value of the latter depends on the coupling strength of the magnetic impurity with the metal. The larger is the surface-impurity coupling, the broader the resonance will be.

The Kondo regime and its related resonance ZBP only exist for values of the side peaks' width that do not overlap. That is:  $\epsilon_0 \gg \Gamma$ ,  $U \gg 2\Gamma$ . In the case  $\epsilon_0 \sim \Gamma$ ,  $U \sim 2\Gamma$  the regime enters in the so-called mixed valence regime, where spin fluctuations between the levels  $\epsilon_0$  and  $\epsilon_0 + U$  are possible because these two resonances overlap.

The Kondo temperature,  $T_K$ , reflects the binding energy between the unpaired spin localized at the resonance and the electrons in the metallic reservoir and it is proportional to the width of the ZBP.  $T_K$  can also be related to the parameters of the Anderson model, i.e.  $\Gamma$ ,  $\epsilon_0$  and  $U$  in the following way [174]:

$$T_K = \frac{\sqrt{\Gamma U}}{2} \exp \{ \pi \epsilon_0 (\epsilon_0 + U) / \Gamma U \} \quad (7.1)$$

$T_K$  increases for larger values of  $\Gamma$  and  $U$ . Hence, the strength of the Kondo effect weakens for magnetic impurities better coupled to the host metal or, to a lower extent, with large Coulomb repulsion energies.

To summarize, spin Kondo effect appears if the following conditions are fulfilled: i) there is an electronic level that is singly occupied, i.e., such that  $E_F - U < \epsilon_0 < E_F$  ii) the level is localized, i.e., the Coulomb peaks at  $\epsilon_0$  and  $\epsilon_0 + U$  do not overlap, and iii) the Coulomb peaks have non-negligible coupling with the Fermi sea, i.e., the width of the resonance  $\Gamma$  is finite, not a Dirac-delta function.

An important characteristic of the Kondo effect is a shape dependence of the ZBP resonance with the temperature. For rising temperatures, i.e., increasing fluctuations in the many-body problem, a broadening and a decrease of the ZBP intensity [175, 176, 177] is expected. The relations governing these dependencies are:

- Width of the resonance. The ZBP has the lineshape of a Lorentzian peak where

the Full Width Half Maximum (FWHM) broadens with temperature as [176]:

$$\alpha(T) = 2\sqrt{(\pi k_B T)^2 + 2(k_B T_K)^2} \quad (7.2)$$

where  $\alpha(T)$  is the experimental width of the ZBP (FWHM) including a correction term accounting for the temperature dependence of the Fermi edge and for the lock-in bias modulation effects:  $\alpha(T) = 0.78FWHM + 3.52k_B T + V_{rms}$  [175].

- Intensity of the resonance. The height of the resonance can be fitted with the empirical equation [175]:

$$G(T) = G_0 \left\{ 1 + \frac{T^2(2^{1/s} - 1)}{T_K^2} \right\}^{-s} \quad (7.3)$$

such that  $G(T = T_K) = 1/2 G_0$ . The value  $s$  is a fitting coefficient to the numerical renormalization formalism. In the case of Kondo regime for  $1/2$ -spin system, the value that reproduces numerical renormalization group results is  $s = 0.22$ .

Thus, the study of the lineshape variation with the temperature of the system constitutes i) a proof of the Kondo regime, and ii) the type of Kondo and its strength, via the determination of  $T_K$ .

## 7.2 Kondo effect in an ultra-thin TTF-TCNQ film

Our approach to molecular magnetism is the growth of self-assembled TTF-TCNQ domains with 1:1 stoichiometry in the unit cell. DFT calculations predict the transfer of one electron from TTF to TCNQ and a molecular alignment of the LUMO close to the Fermi level. The electron transferred to TCNQ plays thus the role of the unpaired spin needed to interact with the Fermi sea. The LUMO resonance is the  $\epsilon_0$  level (Fig. 7.1).

In STS spectra the signature of Kondo effect should arise as a feature pinned at the Fermi energy level [178, 179, 180, 181, 182, 183, 184, 185, 186, 187]. The lineshape of the resonance has been identified with a Fano lineshape [182, 188], whose shape varies between a lorentzian peak and a dip. Lineshapes different to a lorentzian ZBP may arise by interference effects between the Kondo channel and other tunneling channels, for example through the organic core of a metal-organic molecule.

Our observations reveal the existence of a sharp quasi-lorentzian resonance centered at the Fermi level (Fig. 7.2(a)) with a width of approximately  $8 \pm 1$  mV. STS performed in the neighboring TTF molecules does not show any special fingerprint at the Fermi level (inset of Fig. 7.2(a)), therefore the signal corresponds unequivocally to the TCNQ molecule located in the self-assembled charge transfer complex. The narrow width of the ZBP rules out the direct association of this peak to a molecular resonance. For comparison, the LUMO of TCNQ embedded in a monomolecular island weakly interacting with the surface presents a width of  $\sim 0.5$  V.

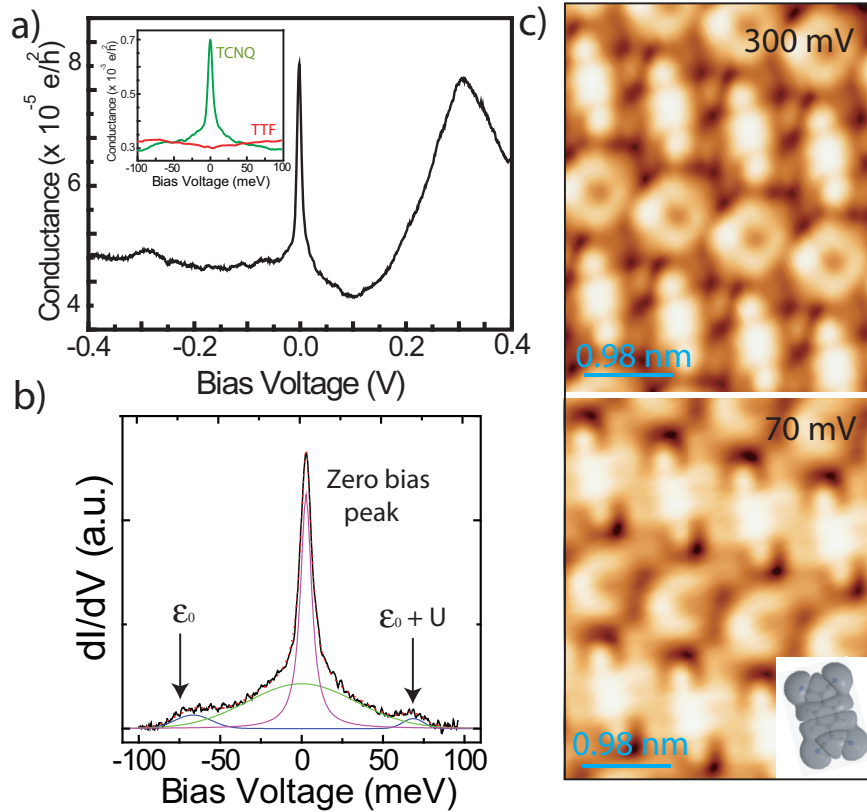


**Figure 7.2:** (a) Large range  $dI/dV$  spectrum, exhibiting both the sharp ZBP centered at zero bias and the hybrid TTF-Au state reported in the previous chapter ( $I = 1\text{ nA}$ ,  $V = 0.4\text{ V}$ ,  $V_{ac} = 1\text{ mV}_{rms}$ ). In the inset a comparison between spectra obtained on TCNQ (green line) and TTF (red line) ( $I = 1\text{ nA}$ ,  $V = 100\text{ mV}$ ,  $V_{ac} = 0.7\text{ mV}_{rms}$ ) is shown. The Kondo effect arises only in the TCNQ molecules. (b) Typical  $dI/dV$  spectrum obtained in a TCNQ molecule. The gaussian fitting enhances the position of both the ZBP at the Fermi level (magenta line) and the satellite Coulomb peaks corresponding to singly and doubly occupied LUMO (blue line). (c) Topography images at bias voltages of 300 mV and 70 mV. The LUMO orbital fingerprint at the cyano groups, missing in the TTF-TCNQ mixed phase for high voltages is recovered at  $eV \sim 70\text{ meV}$ , value of the doubly occupied Coulomb peak. The inset plots the LUMO isosurface of the free TCNQ molecule for comparison.

Two broader resonances (FWHM  $\sim 25\text{ mV}$ ) can be resolved at both sides of the zero bias peak (Fig. 7.2(b)). They are located at  $\pm 67\text{ meV}$ , symmetric with respect to the central peak. Following the scheme in section 7.1, the peak at  $-67\text{ meV}$  corresponds to the energy level  $\epsilon_0$  and its symmetric resonance,  $+67\text{ meV}$ , corresponds to the doubly occupied level  $\epsilon_0 + U$ . Therefore, the value of the Coulomb repulsion in this system is  $U = 134\text{ meV}$ . The symmetry of the CB peaks with respect to  $E_F$  reveals that the LUMO lies in the particle-hole symmetry point. STM images taken at 70 meV reinforces the idea of the molecular origin of the side peaks. The orbital shape at this energy clearly resembles the LUMO of the free TCNQ molecule (Fig. 7.2(c)).

The relation between the Coulomb peaks linewidth  $\Gamma$  and the Coulomb term  $U$  relates this system to a Kondo regime. The sharpness of the ZBP and its pronounced quasi-lorentzian shape reveals that Kondo tunneling, i.e. involving spin-flipping, through the singly occupied level is the main transport channel. The reason lies in a diminished interaction with the underlying surface, due to the lifting of TCNQ from the surface via the interaction with TTF in the formation of the charge transfer complex.

A further verification of the Kondo nature of the ZBP involves the study of its lineshape dependence on the temperature. To do so, the experimental system was gradually heated up from its base temperature, 4.8 K, up to 13.5 K, by shining light inside the STM shield. In this way the STM is slowly warmed up in a controlled way at a rate of, approximately, 0.5 K per 30 minutes. Fig. 7.3 plots the ZBP lineshape for several temperatures and the dependency of both the width (b) and the intensity (c) of the peak on the temperature.

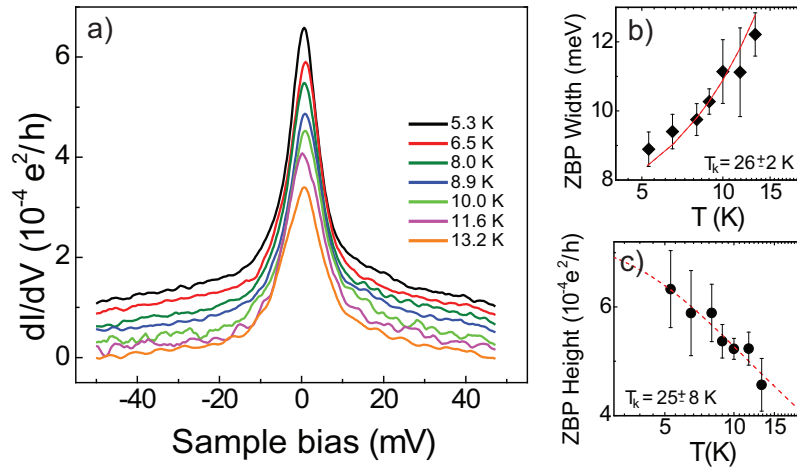


**Figure 7.3:** (a) Lineshape dependence of the zero bias resonance on the temperature ( $I = 0.9$  nA,  $V = 100$  mV,  $V_{ac} = 0.3$  mV<sub>rms</sub>.) The resonance becomes broader and less intense for increasing temperatures. (b) and (c) Behavior of the corrected FWHM ( $\alpha(T)$ ) (b) and the zero bias peak intensity (c) with the temperature. The points are an average over 6-16 measurements per each temperature. The red line fitting follows equations 7.2 for (b) and 7.3 for (c).

The peak width  $\alpha(T)$  (Eq. 7.2), increases with the temperature resulting in a fitted Kondo temperature of  $T_K = 26 \pm 2$  K (Fig. 7.3(b)). This result can be tested with the value yielded by the gradual decrease of the intensity of the ZBP, fitted to the empirical expression of equation 7.3. In this case we obtain a Kondo temperature of  $T_K = 25 \pm 8$  K (Fig. 7.3(c)) in agreement with the fit to the temperature dependence of the linewidth. The good fitting of the ZBP height decrease with the temperature achieved by the empirical equation 7.3 confirms the 1/2-spin origin of the Kondo phenomena. The Kondo temperature reported here is small compared to the 40 K-200 K Kondo temperatures found in organometallic compounds adsorbed on noble metals [179, 180, 185, 186, 187]. In the organometallic compounds the Kondo resonance arises from the

magnetic atom that is attached to the organic molecule. In our case the extra unpaired electron resides in the more delocalized  $\pi$  orbital. Hence, the Coulomb energy is smaller and, in consequence, also  $T_K$ .

### 7.3 Electron-phonon coupling effects on Kondo molecules

The Kondo ZBP exhibits a strong dependence of its lineshape on the STM tip location onto the TCNQ molecule. It reaches its maximum value at the ending cyano groups and decreases gradually while approaching the center of the TCNQ molecule, where it shows its minimum value (Fig.7.4). Together with this decrease of ZBP intensity, two extra side peaks appear at energies of  $\pm 41$  meV, with an intensity comparable to the Kondo resonance at the center of the molecule.

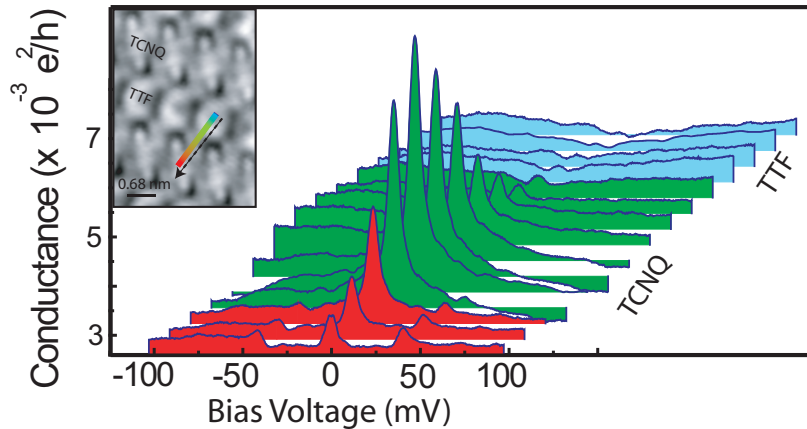


**Figure 7.4:** Plot of 15 spectra taken along a line scan from the center of a TTF molecule to the center of TCNQ ( $I = 1$  nA,  $V = 100$  mV,  $V_{aC} = 0.7$  mV<sub>rms</sub>). The direction of the scan is shown in the inset). The zero bias voltage peak develops on top of the TCNQ, reaching its maximum value at the cyano groups (green curves). Further spectra towards the center of the molecule (red curves) shows the development of extra side peaks at both polarities.

Conductance maps were taken at energies between 5 meV and 150 meV to locate precisely the spatial origin of both the Kondo and the extra side peaks (Fig. 7.5(b)-(i)). While the signal corresponding to the Kondo resonance (Fig. 7.5(b)) belongs to the area close to the cyano group, the signal at 41 meV is more pronounced in the inner part of the TCNQ molecule (Fig. 7.5(d)).

The investigation of transport through molecules addresses the possibility of coupling electronics and vibrations. Molecules have vibrational degrees of freedom which can be excited by charge that tunnels into the molecule [12, 90, 189, 190, 191, 192]. Theoretical predictions describe the viability of an inelastic Kondo effect mediated by vibron-assisted tunneling [193, 194]. The charge tunneling at energies close to the ZBP cause a slight distortion of the molecule and excite vibrational modes (vibronic

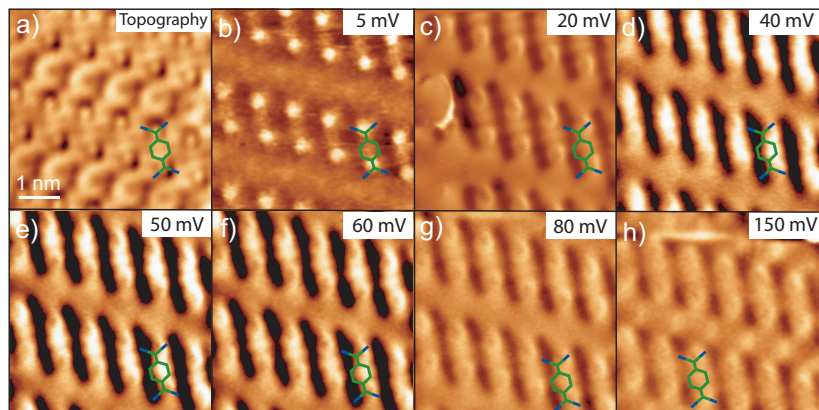


**Figure 7.5:** Conductance maps taken at several bias voltages ( $I = 0.07$  nA,  $V_{ac} = 1$  mV<sub>rms</sub>). The intensity is larger at two energies: at 5 mV (b) the resonance corresponding to Kondo is excited mainly at the area close to the cyano group. Between 40-60 meV (d)-(f) the signal is maximal at the center of the TCNQ molecule. The contrast in the TCNQ molecules decreases for conductance maps taken above this value ((e), (f), (g), and (h)).

coupling). However, the elastic channel remains open and the zero bias resonance is not suppressed by the vibronic coupling but breaks up into vibron side-bands. These satellite peaks represent the resonant tunneling events that involve both spin-flip plus the excitation of a vibration. In our case the symmetric position of the peaks at  $\pm 41$  meV (Fig. 7.6(a)) with respect to the Fermi level and their narrow lineshape constitute a fingerprint of this strong electron-phonon coupling taking place at the center of the TCNQ molecule. The increase of the sidebands is compensated by the decrease of the central ZBP, characteristic of a resonant process.

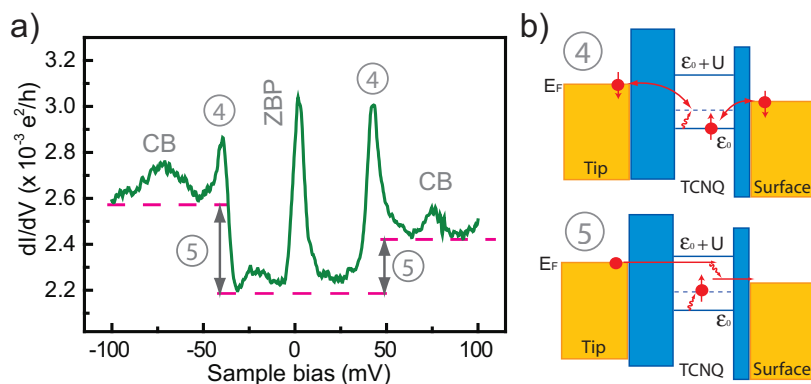


**Figure 7.6:** (a) presents a conductance plot taken on the TCNQ center ( $I = 1$  nA,  $V = 100$  mV,  $V_{ac} = 0.7$  mV<sub>rms</sub>). Two vibrational sidebands (4) arise at  $\pm 41$  meV symmetrically from the diminished zero bias resonance. They involve both spin-flip and excitation of a vibration. The dashed line (5) sketches the characteristic steps of a non-resonant electron transfer process. (b) schematizes the processes (4) and (5).

An additional feature in the  $dI/dV$  spectra observed in TCNQ is the emergence of step-like functions for bias voltages larger than the side bands (dashed line in Fig. 7.6(a)). These steps in conductance are characteristic of a non-resonant electron transfer process assisted by the excitation of vibrations during tunneling through a vacuum barrier [191].

The spectroscopic features present at the center of the TCNQ molecule (resonant vibronic sidebands and non-resonant step) exhibit an asymmetry with respect to the Fermi level. The non-resonant step corresponds to an increase of the junction conductivity of  $\sim 15\%$  at negative polarity which is reduced to  $\sim 10\%$  for opposite bias. The vibronic sidebands present an opposite trend: the larger peak is observed at positive bias voltages (Fig. 7.6(a)). This effect can be related to a competition between the two inelastic tunneling events and mediated by an asymmetric linewidth of the Coulomb peaks. At negative bias voltage the Coulomb peak, corresponding to the single occupied molecular level  $\epsilon_0$ , is larger than the  $\epsilon_0 + U$  Coulomb peak at positive voltages. Since inelastic tunneling is enhanced by resonances close to the Fermi level (Fig. 7.6(b)), the step observed at negative voltages is larger in accordance with a broader molecular resonance. As a consequence of the competition between the two phonon-mediated tunneling processes, the vibronic sideband is thus smaller at this polarity. At positive voltages the process is inverted. The doubly occupied Coulomb peak exhibits a smaller linewidth. The non-resonant step is smaller leading to a larger vibronic sideband.

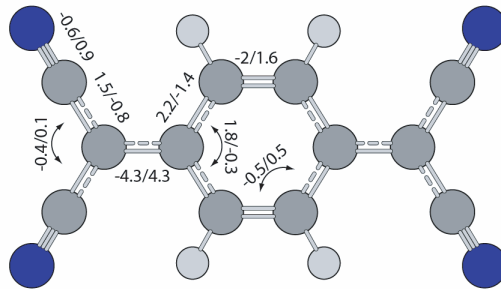


**Figure 7.7:** Structural differences of TCNQ, TCNQ<sup>-</sup> and TCNQ<sup>-2</sup>, minimized by quantum chemistry calculations implemented with the program Gaussian06. The changes in bond length are marked for the TCNQ (left number) and TCNQ<sup>-2</sup> (right number) with respect to the anionic TCNQ<sup>-</sup> state. As a consequence of the charge injection the aromaticity of the central ring increases, becoming fully aromatic for the doubly ionized TCNQ. This is reflected as structural changes of, mainly, the central ring and the exo-ring C=C bonds. Upon addition of electrons, the order of the C=C bonds of the neutral TCNQ is reduced, being this reduction accompanied by an increase of the bond length upon each ionization:  $\sim 4$  pm for the case of the the exo-ring C=C bond, and  $\sim 2$  pm for the ring C=C bond. The TCNQ single C-C bonds of the central ring become shorter with the increasing aromaticity.

The origin of the strong electron-phonon coupling can be understood by an examination of the atomic motion of the vibrational modes exhibited by the TCNQ at

energies close to 40 meV. According to the literature [195, 196], this energy corresponds to a planar breathing mode,  $\nu_9$ , with  $a_g$  symmetry that involves a distortion of the central ring and a stretching of the  $C=C(CN)_2$  double bonds of the  $TCNQ^-$  anion. It is accompanied by a shift of the LUMO position, thus driving charge out/into the molecule. In particular, the  $\nu_9$  mode found here exhibits a large electron-vibration coupling. It fits with the structural distortions undergone by the  $TCNQ^-$  anion upon addition (removal) of charge, namely an increase (decrease) in the aromatization of the central ring and the decrease (increase) of the external C=C bond order (Fig 7.7).

## 7.4 Conclusions

In this chapter we have shown that single molecule magnetism can arise upon charge transfer between non-magnetic molecules. The special mixed organization of TTF and TCNQ on a Au(111) surface provokes the transfer of one electron from TTF to TCNQ. The LUMO of the TCNQ becomes thus occupied and acts as a charge state  $\epsilon_0$  whose spectral fingerprint are the Coulomb peaks. The value of the repulsive Coulombic energy  $U$  and the width  $\Gamma$  of the LUMO at  $\epsilon_0$  is such ( $2\Gamma < U$ ) that the molecular level is singly occupied and the conditions for Kondo effect are fulfilled. A Zero Bias Peak appears thus on the TCNQ molecule at the Fermi level. The analysis of its lineshape dependence on the temperature permits the estimation of a Kondo temperature of 26 K and the confirmation of the spin 1/2 nature of the Kondo effect. This resonance has also a lorentzian lineshape, meaning that the spin-flip tunneling processes are the dominant transport channels at the Fermi level.

The orbital  $\pi$ -character of the  $\epsilon_0, \epsilon_0 + U$  molecular levels together with the presence of molecular vibrations, develops vibration-assisted Kondo fingerprints at the center of the molecule. The intensity of the ZBP varies within the molecule, being maximum at the cyano groups and minimum in the center of the molecular ring. The gradual decrease of the zero bias peak is accompanied by the evolution of two competing phonon-mediated processes. The  $\pi$ -magnetism in TCNQ is a good framework to study the spatial location and the balance of resonant and non-resonant processes.